An empirical re-sampling method on intrinsic mode function to deal with speed variation in machine fault diagnostics

K. S. Wang and P. S. Heyns

Dynamic Systems Group, Department of Mechanical and Aeronautical Engineering, University of Pretoria, Pretoria, 0002, South Africa

Abstract:

Order tracking has proved to be effective in dealing with the effects of speed variation in the analysis of rotating machinery vibration signals. To implement traditional order tracking in practice requires rotational speed information. However, it may be difficult in some cases to mount an appropriate monitoring device to obtain reliable speed information. In this paper, a novel empirical re-sampling of intrinsic mode functions obtained from empirical mode decomposition is explored, so that the approximation of order tracking effects without rotational speed is possible. At the same time, the newly introduced intrinsic cycle concept in the intrinsic mode function simplifies linking of the resultant spectra to signal variations, and is therefore beneficial for condition monitoring of rotating machines. In the paper the rationale behind the technique is first explained. Secondly, the effectiveness of the technique is demonstrated on a dynamic gear simulation model. Lastly, the technique is applied to experimental data from a gearbox test rig. Both the simulation and experimental studies corroborate the usefulness of the proposed technique.

Key words: Empirical Mode Decomposition (EMD), Intrinsic Mode Function (IMF), Order Tracking, Re-sampling, Rotating machinery, Rotational speed.

1. Introduction

Rotating machinery vibration signals often suffer from the effects of variation of the rotational speed. Order tracking techniques were therefore developed to deal with these influences. In recent years, various classes of order tracking techniques have been developed and applied. These include computed order tracking which transforms time domain signals into the angle domain, Vold-Kalman filter order tracking which extracts each individual order or orders from the time domain, etc. To implement traditional order tracking one needs to capture vibration and rotational speed signals simultaneously. The vibration signals are usually measured by accelerometers while the rotational speed signals are captured by tachometers. However, direct measurement of speed may sometimes be difficult due to the complexities of the

machine, e.g. inaccessible gearboxes inside a machine. Thus, the analyst sometimes has to compromise on accuracy for simplification of the system. Furthermore, reliable order tracking (such as Vold-Kalman filter order tracking) requires experience and sufficient mathematical background to support the analysis. These factors may also impede the advancement of order tracking in practice. Simplified signal processing methods to achieve order tracking effects in practical application on real rotating machines might be very beneficial. Thus, it is reasonable to explore the possibilities of using other signal processing methods without the involvement of rotational speed to approximate the effects of order tracking on rotating machine vibration signals.

Vibration signals from rotating machinery may in general be non-stationary and nonlinear. In the literature, a number of techniques have been proposed to deal with such signals. These include techniques to deal with the effects of frequency variation (such as order tracking [1]), modeling techniques for diagnosis (for example cyclostationary modeling [2]) and statistics based methods to detect and characterize non-stationarity (for example spectral kurtosis [3]), as well as time–frequency domain methods to capture the variation of signals with the time (for example the wavelet transform). Various techniques have been developed, but few can deal with both non-stationary and nonlinear signals properly.

In 1998 Huang and his colleagues [4] developed a method that can deal with both non-stationary and nonlinear signals and is known as empirical mode decomposition (EMD). It is an adaptive and unsupervised method with which complicated signals can be separated into a collection of intrinsic mode functions (IMFs) in the time domain. IMFs have been proved to have the ability of capturing useful vibration signals for rotating machine fault diagnosis (see for example [5], [6] and [7]). However, due to the possible frequency variation of IMFs, signal processing techniques that are dependent on Fourier analysis will also be influenced by smearing of the spectra. Specifically for rotating machine vibration signals, the speed variation effects would therefore still remain in the IMFs. Thus, order tracking analysis of IMFs will naturally enhance the diagnostic ability. Since there is no need for rotational speed information in the EMD process, this does however provide possibilities to simplify the order tacking analysis based upon it.

In this paper, a novel way of reconstructing IMFs from EMD to approximate the effect of computed order tracking for rotating machine vibration signals is proposed. In stead of using traditional speed information to achieve the order tracking, an empirical re-sampling method is used on the IMFs which approximates the order tracking effects. Avoiding the need for speed information largely simplifies the practice of signal measurement and the method offers an alternative condition monitoring tool. Besides, the proposed method uses IMFs in stead of complicated raw signals. The simple data structure of IMFs offers additional advantages over the traditional signal processing method in the frequency domain, in that more direct connection between the frequency spectra and signal variations can be obtained. This

will be further explained in the next paragraph. In the following, the first part of the paper explains the rationale behind the technique. Subsequently a simplified gear mesh model is used to demonstrate its ability in simulation studies. Lastly, real experimental gearbox data is studied and demonstrates the ability of the technique in condition monitoring.

2. Basic rationale

Three aspects of the proposed method are now discussed:

a. Reconstruction of newly introduced intrinsic cycles to approximate computed order tracking effects.
b. Interpretation on the reconstructed IMF result.
c. Discussion on the proposed method in terms of rotating machine vibrations.

2.1 The idea of an intrinsic cycle and approximation of computed order tracking effects

Reconstruction of IMFs from EMD is first discussed. Huang et al. [4] define an IMF as a signal that satisfies two conditions:

1) Over the whole signal segment, the number of extrema and the number of zero crossings must be either equal or differ at most by one.
2) At any point, the mean value of the envelope defined by the local maxima and the envelope defined by the local minima is zero.

From this original definition of an IMF, it can be inferred that each IMF is a symmetric and zero mean oscillation wave. This excludes two or more peaks within two successive zero crossings. However, the definition does not ensure that the frequency content of this symmetric oscillation wave is constant. Since the important purpose of computed order tracking is to exclude frequency variation from the rotational speed, it is, therefore, worthwhile to further investigate IMF signals with regards to the effects of frequency variation.

2.1.1 Introduction to intrinsic cycle

The intrinsic cycle (IC) is now introduced. Based upon the idea of an IMF, one may consider a symmetric oscillation wave about a zero mean and define the IC as follows:

Start from the first zero crossing of an IMF and consider two successive zero crossings. The entire signal within these three zero crossings constitute one intrinsic cycle. In the same way, the signal from the last zero crossing of a previous intrinsic cycle and including the following two successive zero crossings, constitute another
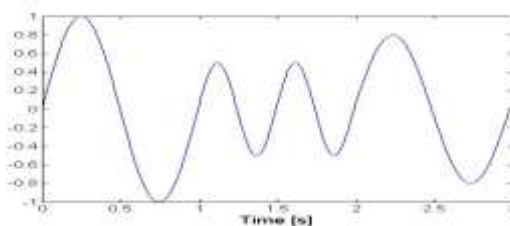
intrinsic cycle, and so on.

The above definition of an IC from an IMF implies that there are one maximum, one minimum and three zero crossings within each IC. Each IC roughly resembles one period of a sine wave. Then considering about frequency variations in terms of newly introduced ICs in an IMF, in these approximately sinusoidal natured ICs frequency variations are not constrained. Variations may exist within and between ICs. If the frequency variation of a signal is solely due to the varying rotational speed, order tracking effects can be achieved by eliminating the frequency variations of the ICs. Thus, this is discussed below by considering frequency variations within and between ICs in an IMF.

2.1.2 Approximation of computed order tracking effects

In computed order tracking [1] the assumption is usually made that the rotating shaft angular acceleration is constant or zero over one revolution, since large angular accelerations or decelerations are usually undesirable in practical machines. This is typically done in commercial software [8]. When there are several ICs within one revolution, one could also assume angular acceleration within an IC is zero so that frequency variations within the ICs may be considered negligible. If this assumption is made and a constant rotational frequency within an IC is therefore implied, the focus in dealing with frequency variation effects may then shift to the frequency variations between ICs.

One can now get rid of the frequency variations between ICs by re-sampling with an equal number of intervals within every IC. The frequency variations between ICs may therefore be discarded and render re-sampled intrinsic cycle data. This process is illustrated in Figure 1 for an arbitrary intrinsic mode function - a non-stationary sine wave.
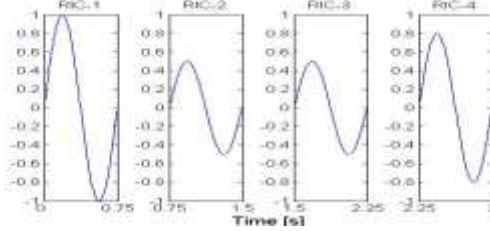

a. An Intrinsic Mode Function
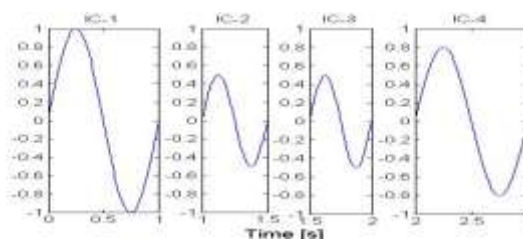
b. Intrinsic Cycles
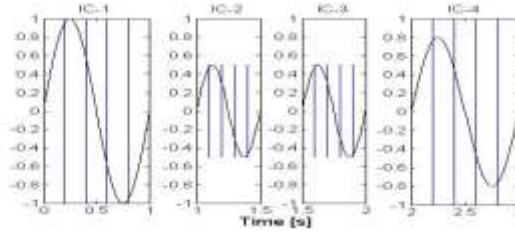
c. Re-sampling

d. Re-sampled Intrinsic Cycles

Figure 1: Illustration of re-sampled IC

For this illustration, an arbitrary IMF sine wave is separated into four individual ICs based upon the definition presented above. It can be seen that the periods of these ICs are different. The 1st (IC-1) and 4th (IC-4) ICs have the same period of 1s but different amplitudes and 2nd (IC-2) and 3rd (IC-3) ICs have the same period of 0.5s and the same amplitudes. This causes the non-stationarity of the signal. These signals are re-sampled into 100 equal intervals within each IC. (In order to clearly illustrate the process visually, only 6 lines are drawn in the figure (c) for each IC and within each line drawn there are 20 equal intervals.) Once the re-sampling is finished, the final wave is reconstructed and features the re-sampled ICs as are shown in (d) which have the same number of equal intervals in each re-sampled IC and each re-sampled IC has the same new period of 0.75s.

The re-sampled ICs have the same periods because each IC has been re-sampled with same number of intervals and a new sampling frequency can be obtained as,

$$f_{new} = \frac{S_{resample}}{t_{period}}$$

(1)

where f_{new} is the new sampling frequency, $S_{resample}$ the number of samples of the re-sampled IMF and t_{period} is the time period of the original data.

Clearly, through this re-sampling process, the frequency variations between the ICs are eliminated. Subsequent to obtaining the re-sampled ICs, it can be seen that if frequency variations within ICs are negligible, which follows on the above zero angular acceleration assumption, then frequency variations of the overall signal are

excluded in a way similar to eliminating frequency variations during computed order tracking re-sampling. For computed order tracking, the non-stationary time domain data is transformed into stationary angle domain data. In this method, a frequency varying IMF is transformed into a frequency stationary IMF. In this way, rotational speed variation effects in an IMF are eliminated. Fourier analysis can then be used to transform the re-sampled IMF into the frequency domain. Thus, similar computed order tracking effects are achieved through re-sampling the IMF. More importantly, though the present approach may achieve similar effects as to computed order tracking, it however neither requires a tacho signal, nor does it rely on interpolation of signals as is done in normal order tracking analysis. This method can be called the intrinsic cycle re-sampling method (ICR).

2.2 Interpretation on the reconstructed IMF result

2.2.1 Reconstructed IMF in terms of analytical form

From the above it is clear that ICR is a development of an IMF. To understand the ICR results it is therefore necessary to trace its analytical form from the basic definition of the IMF. From the literature [9], an IMF $s(t)$ can be written in terms of a normalized amplitude modulation part $A(t)$ and an empirical frequency variation part $\phi_e(t)$, in the time domain as in equation (2),

$$s(t) = A(t)\cos\phi_e(t) \tag{2}$$

The ICR method proposed here transforms the possible frequency varied IMF into a frequency stationary IMF (re-sampled IMF). The empirical frequency modulation carrier wave $\cos\phi_e(t)$ in equation (2) is therefore transformed into a stationary carrier wave as in equation (3)

$$s_{ICR}(t) = A_{ICR}(t)\cos(2\pi f_{ICR}t) \tag{3}$$

where $s_{ICR}(t)$ is the re-sampled IMF through ICR, $A_{ICR}(t)$ is the amplitude modulation part of the re-sampled IMF and f_{ICR} is the main frequency of the re-sampled IMF.

Specifically f_{ICR}, the main frequency of re-sampled IMF can be calculated through the ICs as,

$$f_{ICR} = \frac{N_{ICR}}{T_{ICR}} \tag{4}$$

where N_{ICR} is the number of intrinsic cycles of the calculated IMF and T_{ICR} is the time period of the calculated IMF.

2.2.2 Discussions on the analytical form of reconstructed IMF

Through the development of equation (3) from (2), the original empirical IMF becomes more specific than its original form. In equation (3) the parameters of the re-sampled IMF now become the fixed frequency carrier wave at f_{ICR} with amplitude modulation $A_{ICR}(t)$. As a result, the Fourier spectrum for this kind of signal is affected by only the two variables f_{ICR} and $A_{ICR}(t)$. This simplifies the interpretation of the ICR result. Once the calculated time period in equation (4) is selected, the number of intrinsic cycles will determine the main frequency component f_{ICR}.

However $A_{ICR}(t)$ can still vary according to the nature of the signals but its variations will be reflected in the sidebands of the main frequency component at f_{ICR}. Thus, equations (3) and (4) lead to the following guidelines in examining the ICR results:

a) Considering a re-sampled IMF time waveform, when signal amplitude variations occur in the re-sampled ICs but the number of ICs remains the same, equation (3) implies that $A_{ICR}(t)$ changed due to the amplitude variations and f_{ICR} is invariant due to the unchanged number of ICs. Thus the final spectrum of ICR will exhibit sideband variations and a stationary main frequency peak.

b) When the number of ICs varies and the amplitude of re-sampled ICs in the time waveform remains constant, i.e. $A_{ICR}(t)$ is invariant and f_{ICR} changes in equation (3), the final spectrum will exhibit a shift of main frequency peak and stable sideband shapes.

c) When the signal variations influence both the number of ICs and amplitude of re-sampled ICs in the time waveform, according to equation (3) both $A_{ICR}(t)$ and f_{ICR} are varied. One may then expect a shift of the main frequency component as well as a variation in the sidebands.

d) Further, the more the variations of the amplitude modulation $A_{ICR}(t)$ in the re-sampled IMF, the more variations of sidebands will appear in the ICR spectrum. And the larger the number of ICs, the higher the value of the main frequency component f_{ICR} will be.

Firstly, considering rotating machinery faults, incipient machine faults will usually not severely influence the vibration signals, therefore in a re-sampled IMF, one may typically expect variations in the amplitude of the re-sampled ICs without changing the number of ICs. Introduction of a new IC requires at least one extra zero crossing in the signal. A small signal variation in a dominant vibration environment, especially for rotating machine vibrations where rotational speed harmonics are predominant, will not easy to introduce extra IC due to small variations of the signal. Thus, it may only change $A_{ICR}(t)$ and the main frequency component, f_{ICR}, will remain the same.

In such a case, the sidebands of the ICR spectrum relative to the main frequency component amplitude can be used for condition monitoring purposes. This corresponds to case (a).

Secondly, if the measured response on the machine does not contain clear machine fault vibrations but only influences from the changes in rotational speed which leads to variations of ICs, f_{ICR} will however shift in the ICR spectrum but the sidebands will retain its original shape. This can be used to detect the influence of rotational speed on the measured signals. This corresponds to case (b).

Lastly, when severe changes in the sidebands and a clear shift of f_{ICR} occur, it usually indicates a machine fault occurred and is developing. This corresponds to case (c). In each condition mentioned in (a), (b) and (c), the severity of signal variations will influence the spectrum of ICR results differently in sidebands, main frequency component or both. This is relevant to case (d).

2.3 Further discussions on Intrinsic Cycle Re-sampling (ICR) method in terms of rotating machine vibration signals

For rotating machinery the order components will usually dominate the response. EMD can empirically decompose these orders into different IMFs. These characteristic orders in different IMFs usually have different physical meanings relating to machine conditions. Thus, each IMF is of great use in condition monitoring, and therefore ICR on IMF will also have advantages in this regard. Ideally, one IMF should capture one order signal and represent one single order component in the order

spectrum, as implied by the word 'intrinsic'. However, the IMF may also include other components due to its empirical nature. And the more other components appear in the IMF, the more pronounced the deviations from the order signal will become. As such the final Fourier spectrum of this IMF may contain more variations. This is in fact extremely useful for fault diagnosis of rotating machines, since most of the machine fault vibrations would modulate the order signals. And the IMF has the ability to include this information together with the order of interest.

Researchers such as Feldman [10] have discussed the resolution of the EMD method. They proved that one IMF may include more than one harmonic signals and signals with small amplitudes compared with the dominant harmonics, may easily be included in an IMF. Wang and Heyns [11] also prove this opinion in their simulation and experimental studies on application EMD method in rotating machine vibration signals. While this is actually a disadvantage of IMF in extracting solely order signals, compared to conventional order tracking techniques, it does however provide a unique ability for capturing signals that modulate dominant order signals. Thus, ICR developed from IMFs can be used as a tool to reflect changes of vibration signals that modulate order signals. It could be very useful for condition monitoring of rotating machinery. In the following a simplified gear mesh model is used to demonstrate ICR. The logic of performing ICR is first schematically summarized in Figure 2.
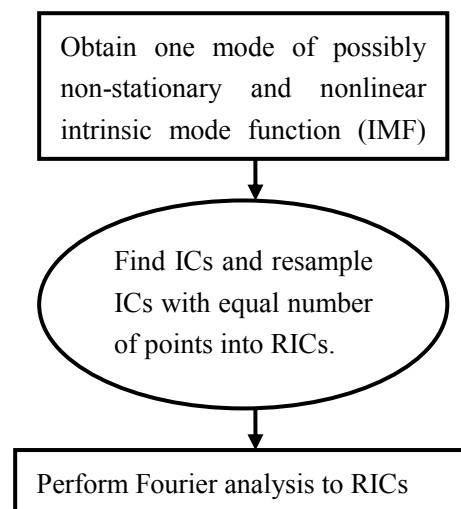
Obtain one mode of possibly non-stationary and nonlinear intrinsic mode function (IMF)

Find ICs and resample ICs with equal number of points into RICs.

Perform Fourier analysis to RICs

Figure 2: Schematic of ICR logic

3. Simplified gear mesh model study

3.1 Gear mesh model

A simplified gear mesh model shown in Figure 3 is used for the simulation study. This model was also used by Stander and Heyns [12] to investigate the advantages of instantaneous angular speed for gearbox condition monitoring. It is adopted here to obtain simulated gear mesh signals. The model comprises four degrees of freedom. A unique

feature of the model is the incorporation of a translating mass M_1 to represent conventional translational vibration monitoring on the gear case. Model characteristics are given in Table 1.
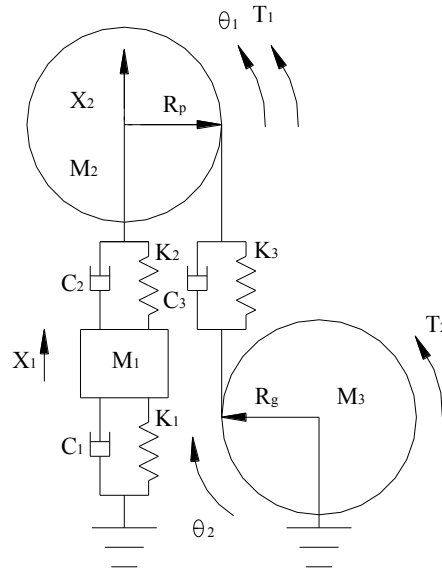

Figure 3: Dynamic gear mesh model

Table 1 Model characteristics and system load

M_1	Translating mass	0.05 kg
M_2	Pinion mass	0.05 kg
M_3	Gear wheel mass	0.05 kg
I_1	Inertia of pinion gear $I_1 = \dfrac{1}{2} M_2 R_p^2$	$2.5 \times 10^{-6} kg \cdot m^2$
I_2	Inertia of gear wheel $I_1 = \dfrac{1}{2} M_3 R_g^2$	$2.5 \times 10^{-6} kg \cdot m^2$
K_1	Structural damping	100 kN/m
K_2	Bearing stiffness	100 kN/m
K_3	Gear mesh stiffness	$100\{1 - 0.01\sin(N \times \theta_1)\}$ kN/m
C_1	Structural damping	1.2 Ns/m
C_2	Bearing damping	1.2 Ns/m

C_3	Gear mesh damping	1.2 Ns/m
R_p	Pinion base circle radius	0.01 m
R_g	Gearwheel base circle radius	0.01 m
N	Number of gear teeth	10
GR	Gear ratio	1:1
f_s	Sampling frequency	8192 Hz
I	Number of re-sampling intervals within one revolution	2000
Input torque	$T_1 = 1 + 0.1\sin\omega t$, $\omega = 2\pi \times 25$	
Load	$T_2 = K_s \dot{\theta_2}^2$, $K_s = 16.2$	

The gear mesh stiffness K_3 is modeled to allow a 2% sinusoidal variation of the nominal gear mesh stiffness so as to simulate the fundamental gear mesh harmonic. This is based upon the work of Howard et al. [13]. A simple viscous damping model is assumed.

A unity input torque T_1 is applied to the input pinion of the model with a 20% variation in time in order to simulate the fluctuating input and therefore causes the variations of rotational speed. The load on the system is set proportional to the square of the gearwheel speed, which enables the system to accelerate up to a nominal speed during the simulation. A proportional constant K_s is chosen to control the resultant nominal steady-state rotational speed of the system. Choosing K_s = 16.2, one obtains a nominal system rotational speed of 1500 rpm. The equations of motion describing the model are presented in Eqs. (5) – (8)

$$M_1\ddot{X}_1 + (C_1 + C_2)\dot{X}_1 + (K_1 + K_2)X_1 - C_2\dot{X}_2 - K_2X_2 = 0 \tag{5}$$

$$M_2\ddot{X}_2 + (C_2 + C_3)\dot{X}_2 + (K_2 + K_3)X_2 - C_2\dot{X}_1 - K_2X_1 - C_3R_g\dot{\theta}_2 \tag{6}$$

$$- K_3R_g\theta_2 + C_3R_p\dot{\theta}_1 + K_3R_p\theta_1 = 0$$

$$I_1\ddot{\theta}_1 + R_p^{\,2}C_3\dot{\theta}_1 + R_p^{\,2}K_3\theta_1 - R_pR_gC_3\dot{\theta}_2 - R_pR_gK_3\theta_2 + R_pC_3\dot{X}_2 + R_pK_3X_2 = T_1 \tag{7}$$

$$I_2\ddot{\theta}_2 + R_g{}^2C_3\dot{\theta}_2 + R_g{}^2K_3\theta_2 - R_gR_pC_3\dot{\theta}_1 - R_gR_pK_3\theta_1 - R_gC_3\dot{X}_2 - R_gK_3X_2 = T_2 \quad (8)$$

The model was written into state space format and implemented in MATLAB for simulation with the ode45 differential equation solver.

3.2 Application of ICR on simulation environment

In this simulation studies, the ICR technique will be tested. To implement ICR technique, one should first find a proper IMF which could be used for condition monitoring purposes, thereafter ICR procedure could be applied on the IMF. Once the proper IMF is chosen, the ICR result will be used to explore two questions in this simulation study:

    a) How does the ICR result relate to order analysis in the simulation model?
    b) How does ICR perform as an alternative condition monitoring tool?

3.2.1 Choosing an appropriate IMF

Before the above questions can be addressed, the first step is to choose an appropriate IMF for the analysis. To do this the relationship between the original gear casing velocity signal $\dot{X}_1$ and its IMFs is first considered. For this purpose the gear response was simulated over a 5 s period. The last 1 s of this response, after steady conditions have been reached, is now considered in the following analysis. In this steady state the variation of the rotational speed of the gear still remains due to the fluctuating load. For illustrative purposes, a section of 0.25 s of this signal is depicted in Figure 4(a). The low frequency fluctuation at 25 Hz, due to the variation in input torque, can easily be observed in this figure. Higher frequencies are the result of gear meshing which corresponds to 250 Hz (the 10th order) at the nominal rotational speed of 1500 rpm. The response at gear meshing frequency is of great importance for obtaining information about the deterioration of the gear (i.e. stiffness). Basic Fourier analysis is performed in Figure 4(b). Except for the rotational frequency peak at 25 Hz and the gear mesh frequency of 250 Hz, it shows several sidebands around the gear mesh frequency. This is due to the fluctuation of the rotational speed caused by the fluctuating load.
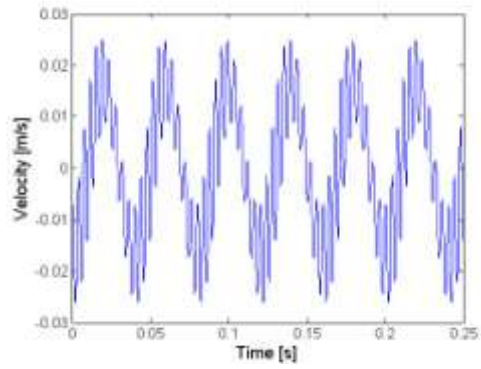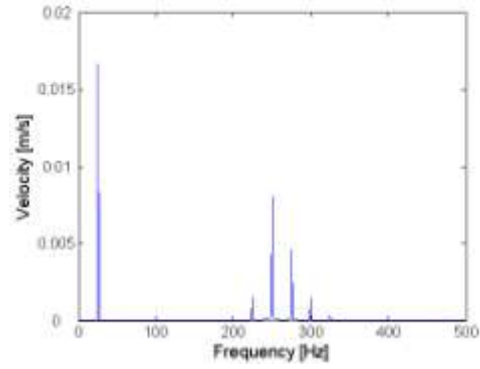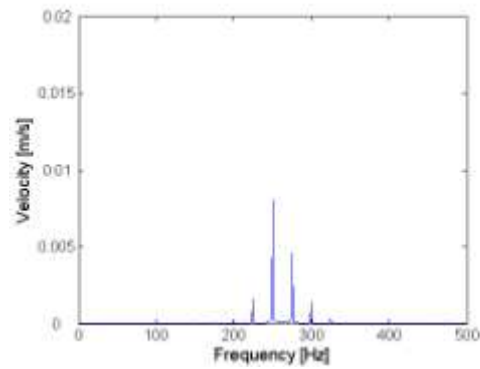
a. Velocity $\dot{X}_1$ b. Fourier spectrum of velocity $\dot{X}_1$
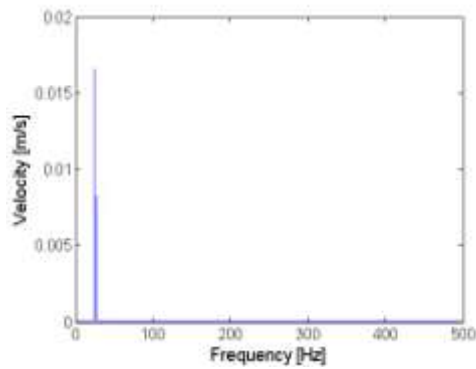
c. Fourier spectrum of 2nd IMF   d. Fourier spectrum of 1st IMF

Figure 4: Velocity $\dot{X}_1$ and associated Fourier spectrum

EMD is now applied to the signal and the spectra of the 1st and 2nd IMFs are plotted in Figures 4(d) and (c) respectively. The 1st and 2nd IMFs successfully separate the lower and higher frequency content. This can of course also be achieved by using low and high pass filters but, in this case is accomplished empirically. The 2nd IMF captures the rotational frequency at 25 Hz while the 1st IMF extracts the gear mesh frequency content and its sidebands. Clearly, the 1st IMF which relates to the gear mesh frequency content, captures the changes of gear stiffness and is therefore the appropriate IMF for further analysis of the ICR method in condition monitoring.

3.2.2 Comparison of ICR result to order analysis in the simulation model

To investigate how the ICR results relate to order tracking analysis in this model, results from conventional order tracking analysis and ICR on the 1st IMF, are compared in Figure 5. Since the 1st IMF is focused on the gear mesh vibrations, the conventional order tracking analysis also focuses on gear mesh vibration for comparative purposes. The 10th order is extracted from the raw signal by

Vold-Kalman filter order tracking (VKF-OT), through which the gear mesh order (10th order) is obtained. (A 20% relative filter bandwidth is used. This means that the ratio of the instantaneous absolute filter bandwidth to the instantaneous rotational speed frequency is 0.2. See references [14] and [15] for more details on the choice of the filter bandwidth). Then computed order tracking is applied to the extracted gear mesh order into order spectrum. For further comparison to the ICR results, the figure is normalized in terms of the highest order peak which renders Figure 5(a). The ICR method is applied to the 1st IMF and gives Figure 5(b) which is also normalized in terms of highest frequency peak.

a. 10th order analysis   b. ICR on 1st IMF
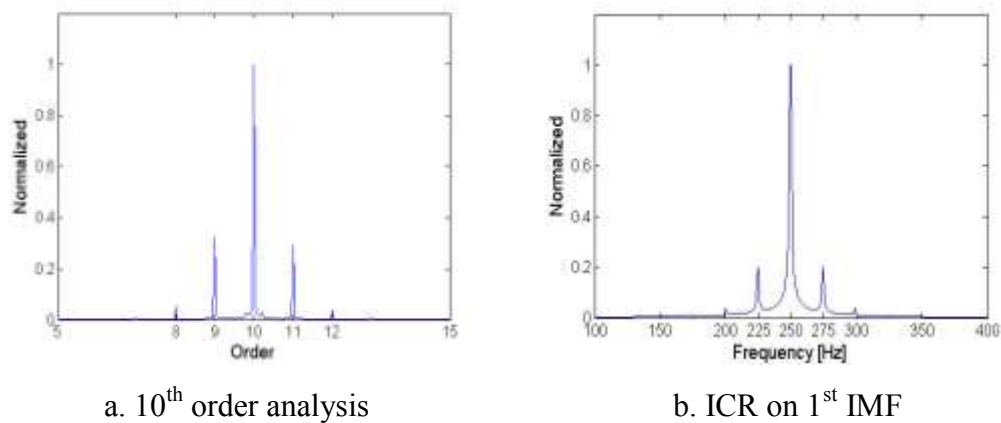
Figure 5: Comparison of COT and ICR results

Through comparison of Figures 5(a) and (b), it is firstly clear from the abscissa that unlike order tracking analysis in Figure 5(a), the ICR result remains in the frequency domain, in stead of the order domain, as is shown in Figure 5(b). This is accomplished by employing the new sampling frequency of equation (1).

Secondly, from the two normalized figures it can be seen that both the order tracking and ICR spectral maps feature similar shapes with one main peak and evenly distributed sidebands. For the order map in Figure 5(a), the order sideband spacing is 1 with the 8th, 9th, 11th and 12th orders present. Similarly, the frequency sideband spacing in Figure 5(b) is 25 Hz with peaks at 200 Hz, 225 Hz, 275 Hz and 300 Hz. The 25 Hz corresponds to the nominal rotational speed. However, the ratio of the highest sideband to the main peak between two figures is slightly different. For Figure 5(a) this ratio is 0.3 and 0.2 for Figure 5(b). The difference is due to the decomposition of the 2nd IMF as is shown in Figure 4(c). The 25 Hz amplitude modulation is the same frequency as the nominal rotational speed, which has been partly separated into the 2nd IMF. This reflects the fact that the ICR method is influenced by the decomposition process of EMD. However, both figures share similar attributes in analyzing the order of interest.

Thirdly, the peaks on the order analysis results in Figure 5(a) are sharper than the ICR result in Figure 5(b). This also suggests a difference between the two methods. Firstly,

the original sampling frequency in the simulation was set at $f_s = 8192 Hz$ in Table 1. After re-sampling, the new sampling frequency for the ICR analysis changes to

$$f_{new} = \frac{S_{resample}}{t_{period}} = \frac{48001}{1} = 48001 Hz$$ as defined in equation (1). (In this case, within

a 1 s signal, there are 24 revolutions and 250 intrinsic cycles. The re-sampling interval in one revolution is $I = 2000$ (see Table 1). Thus the number of re-sampled intervals for the computed order tracking analysis is $24 \times 2000 = 48000$. To keep the same number of analysis samples for ICR, 192 intervals within one intrinsic cycle is chosen, therefore, the $f_{new} = 48001 Hz$). And the Nyquist frequency for this ICR analysis

is $f_{Nyquist} = \dfrac{f_{new}}{2} = 24000.5 Hz$. For order analysis, the order sampling frequency is

$$O_{sample} = \frac{1}{2\pi/I} = \frac{1000}{\pi} = 318.3 \quad \text{order} \quad \text{and} \quad \text{the} \quad \text{Nyquist} \quad \text{order} \quad \text{is}$$

$$O_{Nyquist} = \frac{O_{sample}}{2} = \frac{500}{\pi} = 159.15 \text{ order.}$$ Considering the ratio of the dominant

components in the order spectrum and the ICR results to their Nyquist values, a difference can therefore be calculated that the dominant nominal gear mesh

vibrations, f_N, in the ICR spectrum occurs at $\dfrac{f_N}{f_{Nyquist}} = \dfrac{250}{24000.5} 100\% = 1.04\%$ of

$f_{Nyquist}$. However for order analysis, the corresponding gear mesh at the 10th order,

occurs at $\dfrac{O_{10th}}{O_{Nyquist}} = \dfrac{10}{159.1} 100\% = 6.29\%$ of $O_{Nyquist}$. Clearly, the ratio of the frequency

components in the ICR spectrum and the order component in order spectrum are different from their Nyquist values. As a result, the order spectrum in Figure 5(a) looks sharper than ICR spectrum in Figure 5(b). This indicates that the new sampling frequency for ICR analysis may influence the visual appearance of the of the spectrum map.

Lastly, it should always be borne in mind that ICR is strictly speaking not an order tracking analysis. It reflects changes of the signal itself. Only when the frequency variation in signals is caused by rotational speed, it may serve as an alternative order tracking approximation. Fortunately, in many practical applications for rotating machine vibrations, such an assumption is applicable. This is the case in this simulation study for gearbox in good condition.

In summary, to make clear of the differences between the two techniques as have been

discussed above, it may use a comparison table to explicit it in Table 2.

Table 2 Comparison between ICR result and order analysis

	Order tracking effects	Spectrum unit	Spectrum Nyquist frequency	Rotational speed info.
ICR technique	Good approximation but influenced by the EMD decomposition process	Frequency	influenced by the number of Re-sampling samples	No need
Order analysis	Good	Order	Influenced by order sampling frequency	Need

3.2.3 Traditional signal processing methods and ICR as an alternative condition monitoring tool on seeded fault

a) Traditional signal processing methods on seeded fault

Subsequently a typical seeded fault is introduced. The gear mesh stiffness K_3 is reduced to 98% of the nominal gear mesh stiffness at an angle from $160°$ to $165°$ of the shaft rotation. Firstly, traditional signal processing methods are applied to the signals from the gearbox in good condition and with the seeded fault so that a clear picture of how traditional signal processing methods respond to the fault can be obtained. Thus, time, frequency and order domain analyses are first compared in Figure 6.
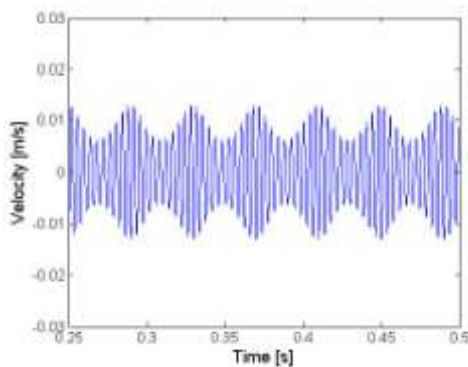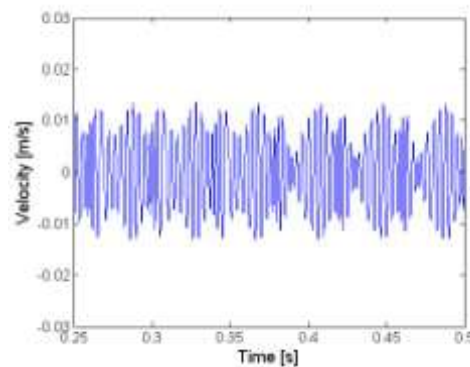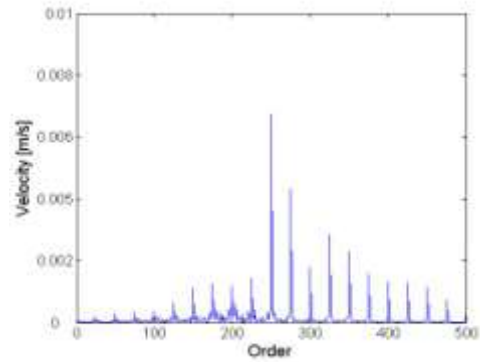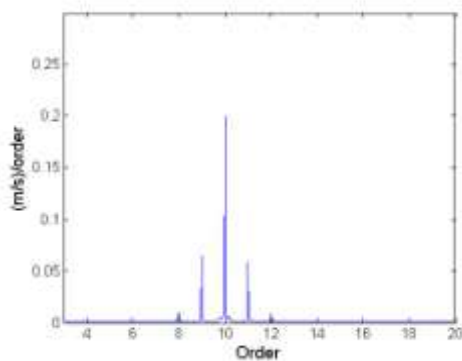

a. 1st IMF for good condition   b. 1st IMF for fault condition
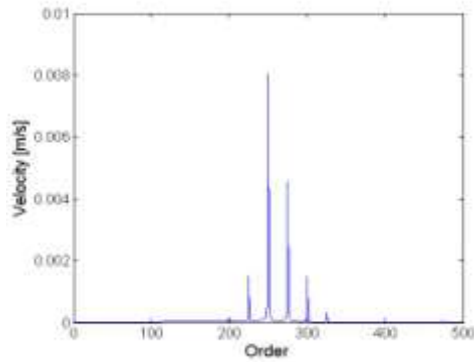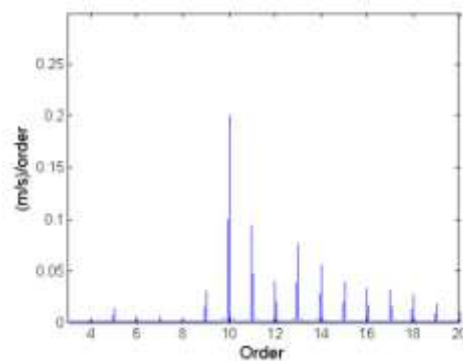
c. FFT on 1st IMF for good condition

d. FFT on 1st IMF for fault condition

e. Order tracking for good condition

f. Order tracking for fault condition

Figure 6: Comparison of good and seeded fault conditions

The 1st IMF time domain velocity signals for good and fault conditions in Figures 6(a) and (b) show that the high frequency gear mesh signal has been extracted from the original velocity. In Figures 6(a) and (b), the amplitude variations are both clearly visible. Comparing the two figures indicate that the gear mesh vibrations change due to the introduction of the fault.

In the frequency domain, Figures 6(c) and (d) show the frequency spectra of the 1st IMF signals. Sideband peaks are very clear in both figures. With the introduction of the fault, the corresponding spectrum in Figure 6(d) shows more sidebands and some of its peak amplitudes change. Figures 6(e) and (f) consider the order domain, to test the ability of the computed order tracking method for raw signals. Compared with Figure 6(d) in the frequency domain, the order domain spectrum features cleaner order components. This is due to the exclusion of speed variation effects. However by the reduction of gear mesh stiffness to 98%, more sidebands and order peak amplitude variations occur. This implies that the order tracking method also detects the changes in the system. In short, it may be noticed that traditional signal processing techniques detect the system changes in terms of amplitude changes in the time domain and peak amplitude changes in the spectrum as well as more sidebands appearance.

**b) ICR as an alternative tool on seeded fault detection**

Unlike the traditional methods discussed above, the way in which ICR responds to the fault, follows the fundamental characteristics of re-sampled IMF as is discussed in paragraph 2.2. The two aspects of the ICR results that respond to the fault are examined, namely the sidebands variation (S.V.) due to $A_{ICR}(t)$ and the value of the main frequency (M.F.) due to f_{ICR}. To trend the changes in the ICR results, a range of six fault conditions are considered. They are 100%, 99.6%, 99.2%, 99%, 98.5% and 98% of the original gear mesh stiffness. The ICR results for these cases are plotted in Figure 7.
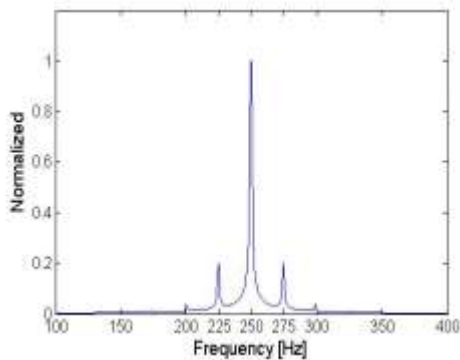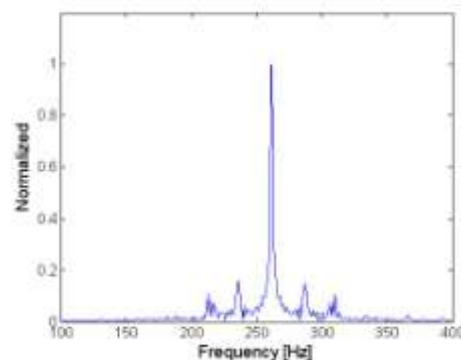

a.100% stiffness (good condition)
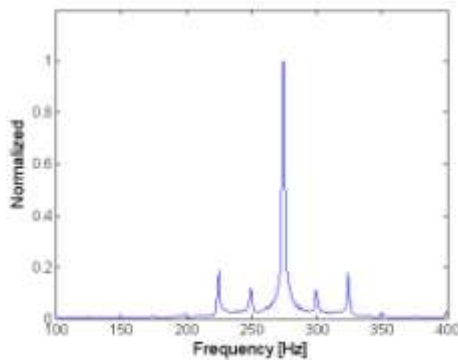S.V.: two clear sidebands and peak ratio 0.2
M.F.: 250 Hz
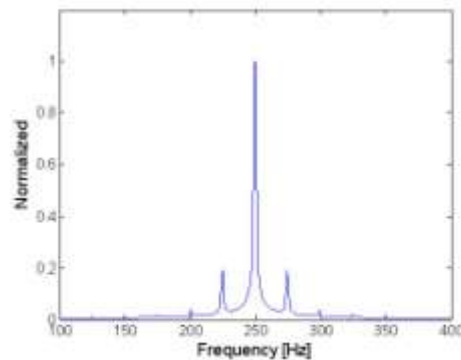
b. 99.6% stiffness
S.V.: two clear sidebands and peak ratio 0.19
M.F.: 250 Hz
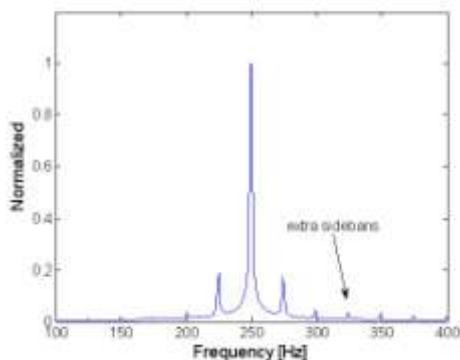
c. 99.2% stiffness
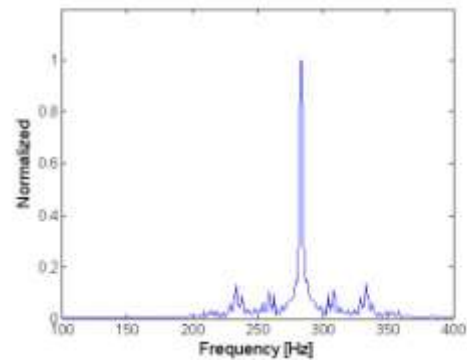S.V.: extra sidebands and peak ratio 0.185
M.F.: 250 Hz

d. 99% stiffness
S.V.: 4 deformed extra sidebands
M.F.: 262 Hz

e. 98.5% stiffness   f. 98% stiffness
S.V.: 4 clear uneven amplitude sidebands   S.V.: more deformed sidebands
M.F.: 275 Hz   M.F.: 283 Hz

Figure 7: ICR results on different fault conditions

Figure 7 shows the variation of the ICR results with the development of the fault. Instead of many sidebands appearing as happens in the frequency and order domains, the two aspects (S.V. and M.F.) show the progress of the fault. For this simulation study, the faults can be categorized into two stages in terms of M.F: Initially (Figures 7(a) to (c)) the M.F. is stationary. For Figures 7(d) to (f) M.F. is varying. This corresponds to point (a) in the guidance provided in paragraph 2.2.

In the first stage, the peak ratio between the highest sidebands to the main frequency peak can be used as a distinct indicator of changes in the signals. The S.V. ratio decreases with the development of the fault from 0.2 to 0.19 and then change to 0.185. This indicates that a variation of $A_{ICR}(t)$ occurs, albeit very small. Considering further the S.V. effects, it can be seen that (especially in Figure 7(c)) extra sidebands grow with the development of the fault. This further confirms that $A_{ICR}(t)$ is varying and it requires more sidebands to represent these changes. Due to the stationarity of the M.F. as well as the above discussions on the changes in S.V., it may be concluded that during the first stage, the fault does not severely influence the 1st IMF or gear mesh vibrations, although it is developing.

In the second stage, the M.F. values may be used as a distinct indicator of the system changes. With the development of the fault, the M.F. becomes 262 Hz, 275 Hz and 283 Hz respectively. It is also found that the sidebands become uneven in amplitude in Figures 7(d), (e) and (f). The shapes of the sidebands become severely deformed in Figures (d) and (f). However, it notices that in figure (e) sidebands are smoother than the other two figures especially it is smoother than figure (d) where the fault on gear mesh stiffness is smaller. In such a case, according to the discussion of paragraph 2.2, M.F. values should be first considered as the indicator of fault severity, despite with

smoother sidebands, figure (e) however shows more serious fault than figure (d) due to the bigger value of M.F. Besides, the smoother sidebands of figure (e) indicates that, compared to the other two fault conditions in (d) and (f), the amplitude part of the re-sampled IMF, $A_{ICR}(t)$, can be represented by much simpler sidebands in (e). In fact, it is an intermediate period of fault development. In such a case, when M.F. is different, the S.V. is not a decisive factor to determine the severity of the fault however M.F. should be first considered. According to theoretical studies in paragraph 2.2 the guidance (c), in this second stage, the seeded faults severely influence the 1st IMF or gear mesh vibrations, the shift of M.F. with severe S.V. indicates a big variation of signals, thus apparently the severity of the damage is increasing.

c) Comparisons of ICR to traditional signal processing methods

In the end, one should compare the differences between the ICR result with traditional condition monitoring methods. The good and fault condition (at 98% nominal gear mesh stiffness) figures are first plotted for comparison. All figures are normalized in terms of highest spectrum peaks in Figure 8.

a. Frequency domain on 1st IMF   b. Order domain
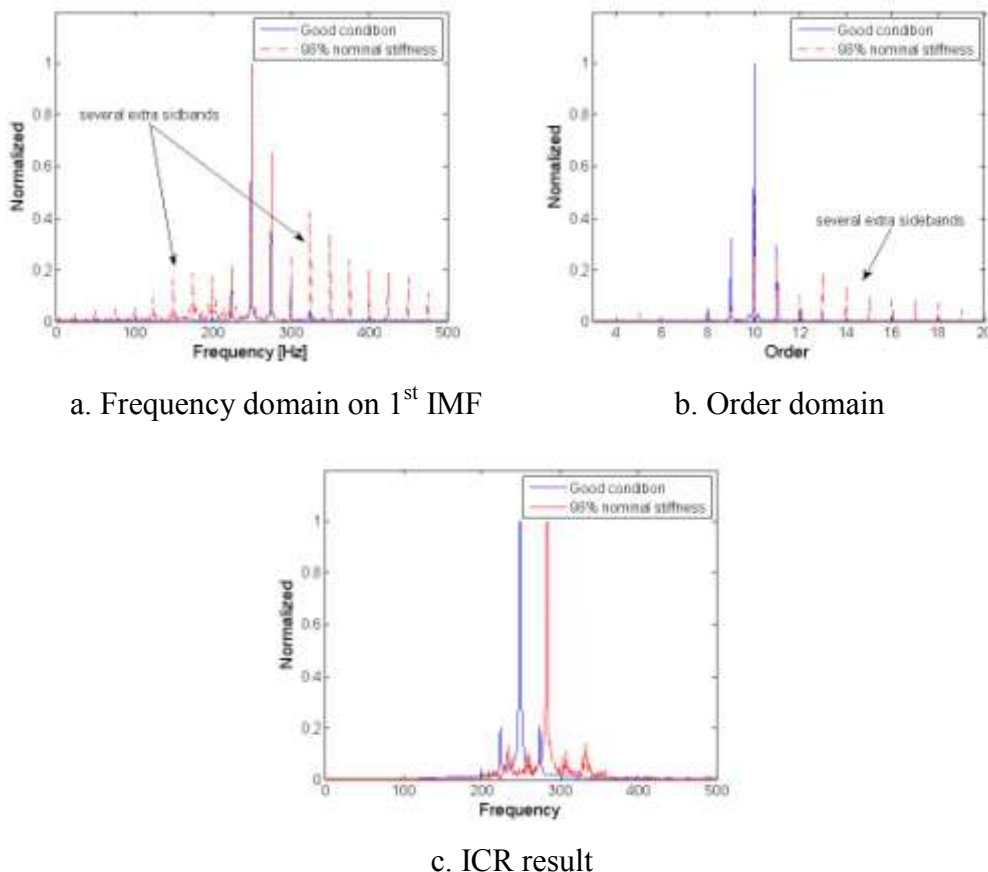

c. ICR result

Figure 8: Comparisons between traditional methods with ICR result

Figure 8 clearly shows that the traditional methods in figures (a) and (b) indicate the

fault is mainly revealed in terms of several extra sidebands as are indicated in both figures. There is significant variation in the frequencies and order peaks. To trend the system changes, one needs to attend to all these peaks. However, instead of presenting several extra sidebands, the ICR technique in figure (c) with its fundamental characters of re-sampled IMF, S.V. and M.F., can be used to trend the changes of system variations. It may be observed that the ICR method also present distinct changes in the results, especially for the unique shift of the M.F., where traditional methods do not have similar indicators. This suggests the ICR technique as an alternative method for machine fault diagnostic with distinct indicators for condition monitoring purposes. To summarize and further clarify the difference, the characteristics of different techniques in condition monitoring are summarized in Table 3.

Table 3 Traditional signal processing methods and ICR in condition monitoring

	Condition Monitoring		
	Indicators	Characteristics	
Traditional signal processing methods (e.g.: Fourier analysis, order tracking)	By using frequency (order) component and sidebands	Advantage	Direct and easy to understand
		Disadvantage and limitations	1) The result is easy to be influenced by different parameters, e.g.: RPM, complicated signals, noise etc. 2) Need extra information e.g. RPM for order tracking analysis
ICR technique	By using Main frequency (M.F.) and Sideband Variation(S.V.)	Advantage	1) Focused, direct and easy to trend the changes of signal 2) Independent of extra information, e.g. RPM
		Disadvantage and limitations	1) Influenced by EMD process to choose proper IMF. 2) Assumption that non-stationarity of signal is caused by speed variation

4. Experimental data analysis

4.1 Experimental set-up and seeded fault

As a further illustration of the ICR technique in condition monitoring, the technique is now demonstrated in a real working environment on signals from an experimental gearbox. The gearbox test rig was designed to conduct accelerated gear life tests on a Flender E20A gearbox under varying load conditions at the University of Pretoria Sasol Laboratory for Structural Mechanics. The experimental set-up consisted of three Flender Himmel Motox helical gearboxes, driven by a 5 kW three phase four pole Weg squirrel cage electrical motor. A 5.5 kVA Mecc alte spa three phase alternator was used for applying the load. The direct current (DC) fields of the alternator were powered by an external DC supply in order to control the load that was applied to the gears. A sinusoidal load with minimum to maximum loads from 7.4 to 14.7 (Nm) was applied to the alternator. Two additional Flender E60A gearboxes were incorporated into the design in order to increase the torque applied to the small Flender E20A gearbox which is being monitored shown in Figure 9(a). During the experimental process, the gear developed severe wear which eventually culminated in several broken tooth and ultimately a stripped gear tooth. The data used in this experimental study is when the first gear tooth is removed. The gear mesh frequency was 215Hz at 5 Hz shaft rotational speed. For details about the test rig the reader may refer to the paper by Stander and Heyns [11]. In this case however the response measurements were taken with a Polytec PDV-100 laser Doppler vibrometer with a 500 mm/s measurement range (see Figure 9(a)). The original shape of the drive gear is shown in Figure 9(b).


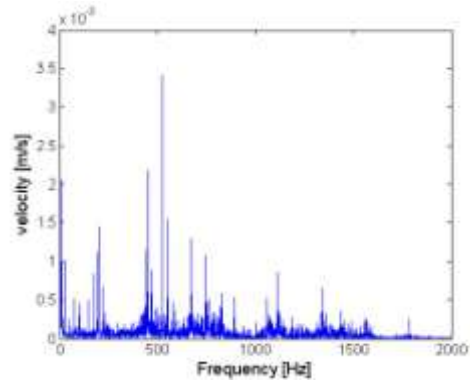a. Experimental test rig of gear box   b. Original status of drive gear
Figure 9: Experimental test rig and gear conditions

4.2 Traditional signal processing analysis on good and seeded fault conditions

The monitored gearbox was set to run at about 300 rpm. To begin with, a 2 s signal was measured before damage was first introduced. The time domain waveform with the corresponding rotational speed, frequency spectrum of the translational velocity and computed order maps around 1× gear mesh order are shown in Figure 10.
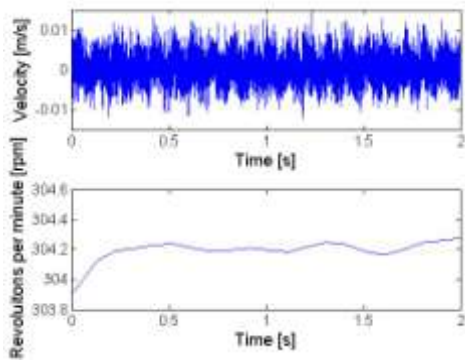
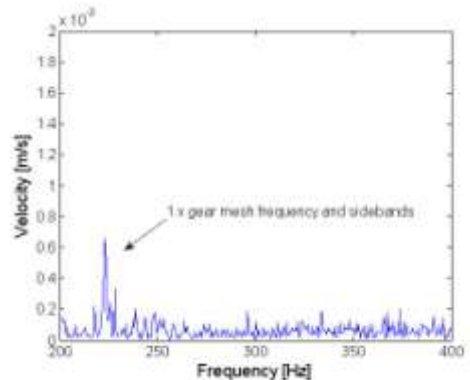a. A typical velocity-time signal   b. FFT on velocity signal
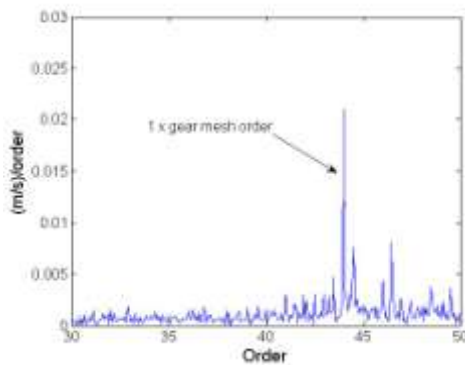

c. Computed order tracking   d. Zoom in for 1× gear meshing frequency

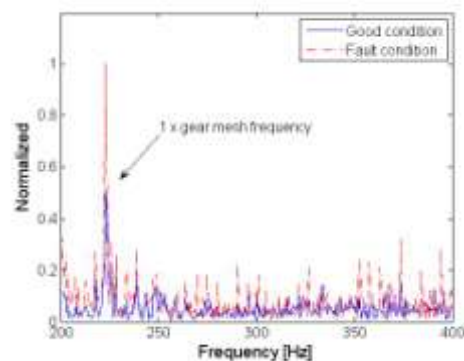Figure 10: Traditional signal processing methods

In these figures no damage has been introduced yet and no clear impacts occur in the time domain signal (Figure 10(a)). However amplitude modulation is visible throughout the period. Although the gearbox operates in a stable condition, the load fluctuation influences the rotational speed which leads to the frequency variation in the signal. From the Fourier analysis (Figure 10(b)) it is clear that the real gearbox data is much more complex than the simulated signal. Many frequency peaks appear throughout the spectrum. For condition monitoring purposes, we focus on the gear mesh frequency in the frequency spectrum. The spectrum after zooming in around 1× gear mesh frequency is shown in Figure 10(d). In figure (d), some sidebands around the gear meshing frequency are also visible which are spaced at approximately 5 Hz. This corresponds to the rotational frequency of the gear. As expected the sidebands for the undamaged gear are few and small. The computed order tracking map in Figure 10(c) which zooms in around 1× gear mesh order is also plotted. It should also be noted that although the order analysis excludes the speed variation effects, the spectra are still fairly complex and show several order sidebands around the gear mesh order.

Once the seeded fault as described in the experimental set-up has been induced, and measured signals are considered over the same period as before. Firstly, traditional signal processing methods are used to detect the system changes. Thus, time, frequency and order domain results are analyzed and compared in different figures as
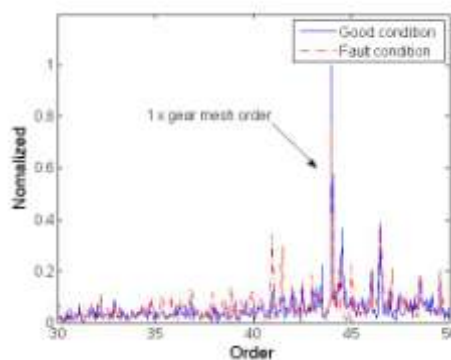
is shown in Figure 11. In order to clarify the differences between figures, good and seeded fault conditions results that in frequency and order domain are superimposed together and normalized in terms of highest frequency or order peaks.
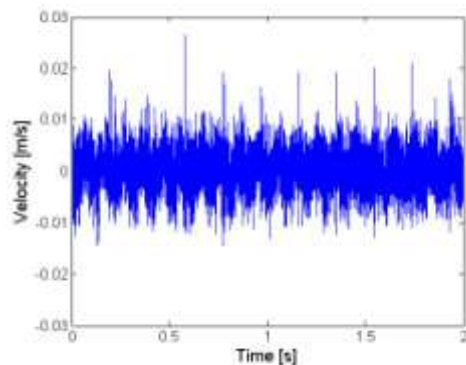
a. Time domain signals(fault)   b. zoomed in 1 × gear meshing frequency

c. zoomed in 1 x gear mesh order

Figure 11: Signals with broken tooth

Firstly, figure 11(a) clearly shows that a periodic impact occurs in the signal, and that the period of this impact is approximately 0.2 second with a corresponding frequency of 5 Hz, which suggests that this impact occurs once per revolution. This is consistent with the induced fault scenario. Secondly, in the frequency domain, it shows that more sharp side bands appear in the spectrum and all the amplitudes of frequency peaks increased, especially the 1× gear mesh frequency component. It is well known that if additional sidebands appear and existing sidebands increase around the gear mesh frequency, this indicates a broken gear tooth problem in the gearbox. Further, computed order analysis comparisons in Figure 11(c) again confirms that extra orders around gear mesh order increased due to the seeded fault on gear teeth, but it also shows that relative amplitude of several order sidebands compared with gear mesh order does not change a lot as happened in frequency domain. However, in this case, the additional order sidebands show the detection of the changes for gear mesh conditions. In short, experimental studies using traditional time, frequency and order domain methods achieve the detection of seeded fault.

4.3 Application of ICR technique

4.3.1 Choosing an appropriate IMF

Once one has a basic understanding of the raw signal, EMD may be applied to the signal to extract the gear mesh information for further ICR application. The 5th to 8th IMFs are plotted in figure 12 as velocity as a function of frequency.

a. 5th IMF   b. 6th IMF

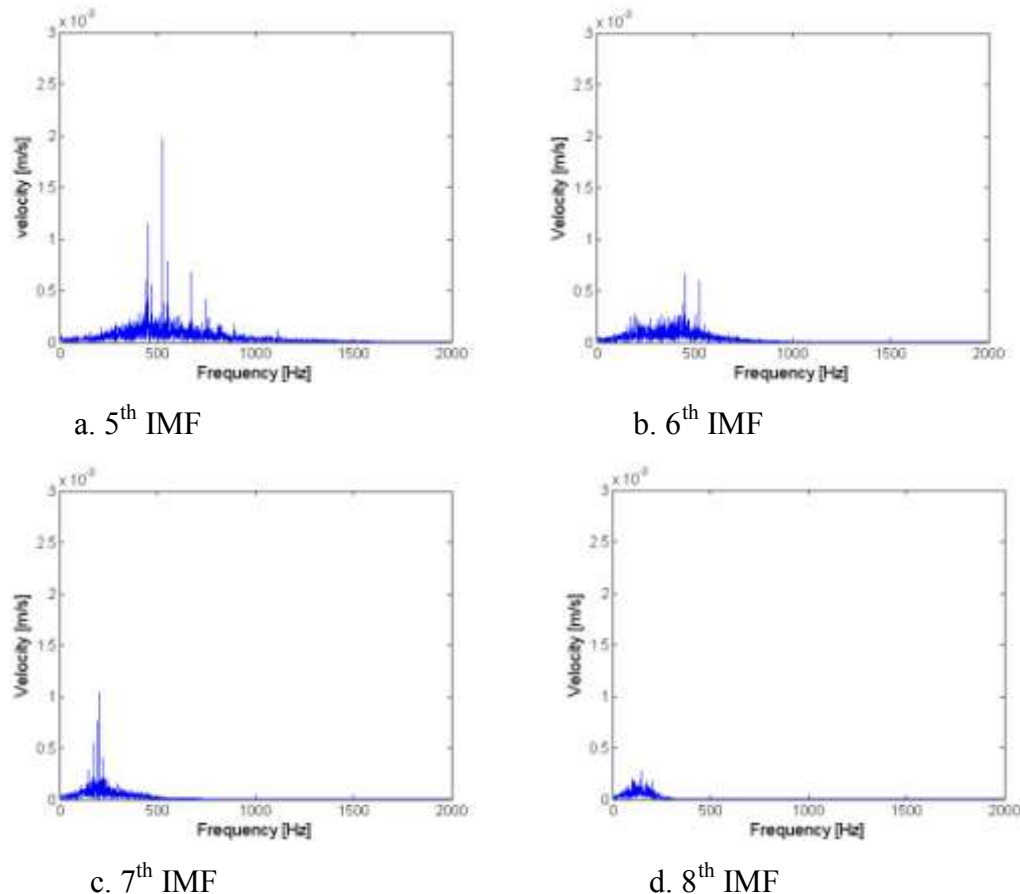c. 7th IMF   d. 8th IMF

Figure 12: IMFs of system response

It can be seen from Figure 12 that the 7th IMF captures the signal content which is relevant to the nominal gear mesh frequency at 215 Hz. Although some energy is present in the 6th and 8th IMF, this is however fairly small. For the 5^{th}IMF very little energy is observed in that range. As a result, the 7th IMF is of great importance for condition monitoring of gear mesh conditions. Therefore ICR is performed on the 7th IMF and result is shown in Figure 13. The result shows that the sidebands around the main frequency peak are oscillating and a clear two distinct sidebands appear around main frequency peak. The whole spectrum only concentrate on frequency range from 150 Hz to 250 Hz in which only those gear mesh related vibrations are being focused. Outside this frequency range, spectrum becomes negligible. This is very different from traditional methods as in Figure 10. In this case, the main frequency component is located at 210 Hz which is very close to the calculated nominal gear mesh frequency at 215 Hz, it is clear that the 7th IMF captures the gear mesh vibrations for
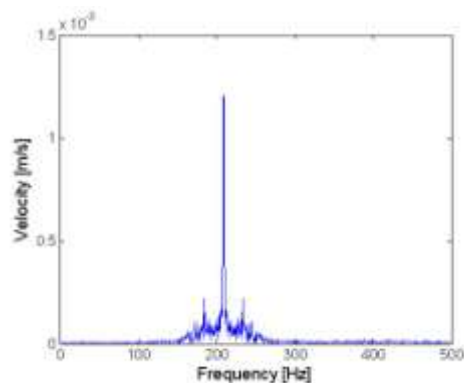
the good condition case data.

Figure 13: ICR on 7th IMF result

4.3.2 ICR technique on seeded fault detection

ICR is then applied to the faulted gear experimental data. In order to clearly show the difference of the spectrum before and after seeded fault, the figure are also superimposed with good condition result and normalized in terms of highest frequency peak. Figure 14 shows the results.
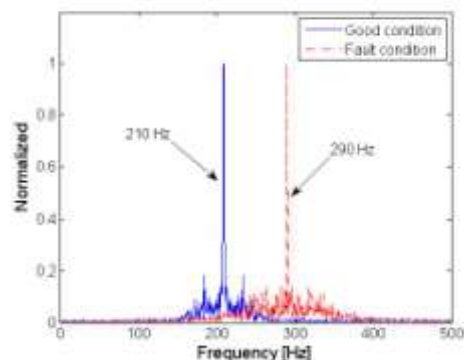

Figure 14: ICR result on faulted gear experimental data

As is argued in paragraph 2.2.2 two aspects of the ICR results respond to faults in the system and are examined in Figure 14, namely Main Frequency (M.F.) and Sidebands Variation (S.V.). Clearly the seeded fault case, the M.F. value has a significant shift from 210Hz in good condition to 290Hz. This is a clear indication of increase of ICs, therefore a shift of f_{ICR}. Then, from the prospective of S.V., firstly, the sidebands changed dramatically, therefore, the variation of the signal could not merely have been caused by rotational speed. This corresponds to paragraph 2.2 guideline (b). Secondly, although the highest sideband amplitudes do not change dramatically relative to the main frequency peak in the fault condition, many more sideband peaks appear in the spectrum. This is very different from good condition where two highest sidebands are distinctly appeared. This indicates that the amplitude modulation part

$A_{ICR}(t)$ of the seeded fault case is fundamentally changed. The above observations correspond to paragraph 2.2 guidelines (c) and (d). Clearly the fault introduced here does not represent a trivial influence to the gear mesh vibrations, which is consistent with the known broken gear tooth damage.

In short, observations from the ICR results clearly show the changes in the gear mesh vibrations. Comparing Figure 11(b), (c) and Figure 14 in frequency, order and ICR results respectively, it is not difficult to obtain that ICR technique provides simple and clear indicators for detecting the changes in terms of M.F. and S.V. especially for the distinct shift of M.F., however traditional methods will present many sidebands and amplitude variations in frequency or order domain which may complicate the process of decision making on fault diagnostic. As a result, compared with traditional methods in fault diagnostic in this experimental study, ICR provides effective and unique indicators for detecting seeded fault which make ICR technique can be a good alternative method to condition monitoring.

5. Conclusion

In this paper, a novel method based on re-sampling of an intrinsic mode function from the empirical mode decomposition method is developed. It is called the intrinsic cycle re-sampling method. The re-sampling process takes advantage of an intrinsic mode function of symmetric, oscillating and zero mean nature to reconstruct an intrinsic mode function into a re-sampled intrinsic mode function which suppress frequency variations of the signal. In this way an approximation of order tracking is obtained without knowledge of the rotational speed. At the same time, it is known that intrinsic mode functions may include non-stationary and nonlinear signals which contain ample machine condition information. Therefore, inherent to the intrinsic cycle re-sampling method developed here, is its ability in condition monitoring. The method further brings advantages for condition monitoring, in that the empirical intrinsic mode function offer specific characteristics for trending. Two parameters are suggested to link signal variations to the final intrinsic cycle re-sampling spectrum map, namely main frequency component and sidebands variations. The simulation and experimental studies both demonstrate that through tracking the changes of these two parameters, intrinsic cycle re-sampling method provides direct and clear connections to signal variations so as to provide a good alternative method for condition monitoring.

Acknowledgments

Reference:

[1]	Fyfe, K. R. and Munck, E. D. S., Analysis of computed order tracking. *Mechanical Systems and Signal Processing,* 11(2), 1997, pp.187-205.
[2]	Antoni, J., Bonnardot, F., Raad, A. and Badaoui, M. EI, Cyclostationary modeling of rotating machine vibration signals. *Mechanical Systems and Signal Processing,* 18, 2004, pp.308-331.
[3]	Antoni, J. and Randall, R. B., The spectral kurtosis: application to the vibratory surveillance and diagnostics of rotating machines. *Mechanical Systems and Signal Processing,* 20, 2006, pp.187-205.
[4]	Huang, N. E., Zheng, S., Long, S. R., Wu, M. C., Shinh, E. H., Zheng, Q., Yen, N. C., Tung, C.Ch. and Liu, H. H., The empirical mode decomposition and the Hilbert spectrum for nonlinear and non-stationary time series analysis. *Proceedings of Royal Society of London* A, 454, 1998, pp.903-995.
[5]	Wu, F.J. and Qu, L.S., Diagnosis of subharmonic faults of large rotating machinery based on EMD, *Mechanical Systems and Signal Processing*, 2009, 23(2), pp.467-475.
[6]	Gao, Q., Duan, C., Fan, H. and Meng, Q., Rotating machine fault diagnosis using empirical mode decomposition *Mechanical Systems and Signal Processing,* 2008, 22, pp.1072-1081.
[7]	Liu, B., Riemenschneider, S. and Xu, Y., Gearbox fault diagnosis using empirical mode decomposition and Hilbert spectrum, *Mechanical Systems and Signal Processing,* 2006, 20, pp.718-734.
[8]	Vibratools. MATLAB toolbox. Axiom EduTech, Sweden, 2005.
[9]	Yang, Zh. J., Yang , L. H., Qing, Ch. M. and Huang, D., A method to eliminate riding waves appearing in the empirical AM/FM demodulation, *Digital Signal Processing,* 2008, 18, pp.488-504.
[10]	Feldman, M., Analytical basics of the EMD: Two harmonics decomposition, *Mechanical Systems and Signal Processing,* 2009, 23, pp.2059-2071.
[11]	Wang K. S. and Heyns P. S. , Application of computed order tracking, Vold-Kalman filtering and EMD in rotating machine vibration, *Mechanical Systems and Signal Processing,* 25(2), 2011,pp416-430.
[12]	Stander, C.J. and Heyns, P.S., Instantaneous angular speed monitoring of gearboxes under non-cyclic stationary load conditions, *Mechanical Systems and Signal Processing*, 2005, 19, pp. 817-835.
[13]	Howard, I., Jia, S. and Wang, J., The dynamic modeling of a spur gear in mesh including friction and a crack, *Mechanical Systems and Signal Processing*,2001, 15 (5), pp.831-853.
[14]	Wang, K. and Heyns, P. S., Vold-Kalman filter order tracking in vibration monitoring of electrical machines, *Journal of Vibration and Control,* 2009, 15(9), pp.1325-1347.
[15]	Herlufsen, H., Gade, S. and Konstantin-Hansen, H., Characteristics of the Vold/Kalman order tracking filter, *Proceedings of the 17th International Modal Analysis Conference*, Kissimmee, FL, February 8-11, 1999.